CrossMark

Effect of CdTe Back Surface Field on the Efficiency Enhancement of a CGS Based Thin Film Solar Cell

YOUSAF HAMEED KHATTAK [ORCID],[1,2,4] FAISAL BAIG,[1,2] BERNABÉ MARÍ,[1] SAIRA BEG,[3] SYED RIZWAN GILLANI,[2] and TANVEER AHMED[2]

1.—ETS de Ingeniería de Diseño, Departament de Física Aplicada, Universitat Politécnica de Valencia, Camí de Vera, Valencia, Spain. 2.—Department of Electrical Engineering, Federal Urdu University of Arts, Science and Technology Islamabad, Islamabad, Pakistan. 3.—COMSATS Institute of Information Technology Islamabad, Islamabad, Pakistan. 4.—e-mail: yousaf.hameedk@gmail.com

Numerical analysis of the proposed solar cell is based on cadmium telluride (CdTe) and copper gallium sulfide ($CuGaS_2$), also known as CGS, is proposed in this research work. Performance of a CdTe/CGS/CdS/ZnO cell is analyzed in Solar Cell Capacitance Simulator (SCAPS) software, by changing the physical parameters like doping density of acceptor, doping density of donor, absorber thickness and buffer thickness. The cell structure is in the same order as the CGS/CdS/ZnO with CdTe used for the back surface field layer. Power conversion efficiency of the CGS/CdS/ZnO solar cell without CdTe is 10.578% (with FF = 83.70%, V_{oc} = 0.82 V, J_{sc} = 15.40 mA/cm^2) and conversion efficiency of CdTe/CGS/CdS/ZnO is 28.20% (with FF = 77.66%, V_{oc} = 1.22 V, J_{sc} = 29.63 mA/cm^3). The overall investigation and simulation results from the modeling of a proposed device in SCAPS is very useful for the understanding of the fundamentals of photovoltaic devices and gives feedback to engineers and designers for the fabrication of CdTe/CGS based solar cells.

Key words: Numerical analysis, CdTe solar cell, CGS solar cell, photovoltaic cell, back surface field, SCAPS

INTRODUCTION

The energy crisis is the critical problem all over the world because of insufficient production of energy. To complete this shortage of energy, different renewable energy resources are used. Renewable energy resources contribute a significant role to meet the energy demands and to produce energy for loads by reducing cost and losses in distribution areas.[1] Among these resources, the most prominent one is solar photovoltaics (PV). PV solar cells absorb the radiation of sunlight and convert it into electrical energy.[2] Non-crystalline and crystalline photovoltaic solar cells are made from elemental and compound material systems. Materials that exhibit higher conversion efficiencies are of the crystalline

group, but their cost of production is higher than poly and microcrystallines. Research has gained more attention for the poly and microcrystalline family of materials due to satisfactory performance, low-cost manufacturing, reliability and stability.[3]

Thin-film photovoltaic solar cells are very useful for low and large-scale solar cell applications. Semiconductor materials like a-Si: H (amorphous silicon), CIGS (copper indium gallium selenide) and CdTe (polycrystalline cadmium telluride) are used for thin film solar cells.[4–10] For thin film solar cells cadmium telluride (CdTe) is an efficient light absorption material. In the comparison of other thin-film materials, for large-scale production deposition of CdTe is easier and more suitable. For terrestrial applications polycrystalline thin-film photovoltaic solar cells like CdTe, Cu(In, Ga)Se$_2$ (CIGS) and CuInSe$_2$ (CIS), compound semiconductors are important because of long-term stable performance, high efficiency and for low-cost

production potential.[11–15] Due to high absorption coefficients, a thin layer of 2 mm is sufficient to absorb the useful part of the spectrum. Highest record efficiencies of 16.5% for CdTe[16] and 19.2% for CIGS[17] have been achieved. The most promising direct band gap materials used in high performance photovoltaic solar cells are CIGS chalcopyrite semiconductors, which can be tuned 1.1 eV for CuInSe$_2$ and 2.2 eV for CuGaS$_2$. These materials are cost-effective and well-known as they have easy processing.[18] In the performance of photovoltaic devices, the band gap energy of the semiconductor materials plays a significant role in conversion efficiency.[19] According to the Shockley–Queisser limit, the optimum calculated energy band gap of a single band photovoltaic device is 1.4 ev.[20] Therefore, due to their high band gap of 2.2 eV, it is not reasonable to use a CuGaS$_2$ (CGS) thin film as an absorber layer in photovoltaic devices based on one junction.[21] So CdTe is also used as a back surface field (BSF) layer with CGS in a proposed solar cell. For enhancing the efficiency of CGS solar cells, a new device is proposed, having two p-type layers stacked above each other. The bottom layer is CdTe, this works as a low band gap back surface field layer, whereas CuGaS$_2$ (CGS) works as a high bandgap absorber layer. As from[22] it is clear that CGS alone cannot be used as an efficient absorber layer due to its wide band gap. So, in this work, we proposed a multi bandgap absorber.

Numerical modeling or numerical analysis is an essential tool for the better understanding of the device working parameters. Numerical analysis can play a significant role in the manufacturing and fabrication of efficient photovoltaic devices. Numerical analysis of multiband-gap absorber CdTe/CGS/CdS/ZnO photovoltaic cells is proposed in this work. Numerical modeling can be done by using SCAPS software. The performance of solar cells is affected from different parameters as are also explained. The band gap of a CdS absorber layer is greater than a CGS absorber layer, so maximum photons are absorbed in the CGS absorber layer. Open circuit voltage (V_{oc}) of a thin film solar cell is increased due to the absorption of photons, which increases the overall conversion efficiency of solar cells. The proposed results will give a valuable guideline for the designing and fabrication of high performance CGS based thin film solar cells.

SOLAR CELL DESIGN AND SIMULATION MODEL

The proposed structure of CdTe/CGS/CdS/ZnO photovoltaic solar cells is shown in Fig. 1. The solar cell structure is based on CdTe (cadmium telluride) and CGS (CuGaS$_2$, copper gallium sulfide) binary compounds as the absorbers and ZnO as a window layer. Whereas a CdS binary compound semiconductor is the buffer layer. This work is carried out to numerically analyze the performance parameters of

the photovoltaic solar cell, that consist of stacked CdTe and CGS as absorber layers. SCAPS simulation software is used to analyze the performance of solar cells.[23–25] The analysis is performed on the following parameters: thicknesses and dopant concentrations of BSF, absorber and buffer layers, effect of temperature variations on the performance of the solar cell, spectral response (QE) and the effect of the illumination power of the sun. This analysis helps to achieve a conversion efficiency of 28.20%.

To simulate the photovoltaic solar cell in the Solar Cell Capacitance Simulator (SCAPS), developed by University of Gent, is used for the modeling of the device. This is a one-dimensional simulation program, and it helps to analyze the spectral response (QE) of a device, $J - V$ characteristics curve, ac characteristics ($C - V$ and $C - f$), energy bands of materials used in solar cells, the concentration of different material used, open circuit voltage (V_{oc}), short circuit current (J_{sc}), fill factor (FF) and power conversion efficiency (PCE) by solving three basic semiconductor equations, i.e., Poisson's equation, and the hole and electron continuity equation.[26–30]

The measure of a photovoltaic cell quality is the fill factor (FF). FF is premeditated by equating the maximum power (P_{max}) to the theoretical power (P_t) that would be output at both the short circuit current (J_{sc}) and open circuit voltage (V_{oc}) together as given in Eq. 1. The ratio of the energy output from the photovoltaic solar cell to the energy input from the sun is the power conversion efficiency (PCE) and mathematically expressed in Eq. 2.

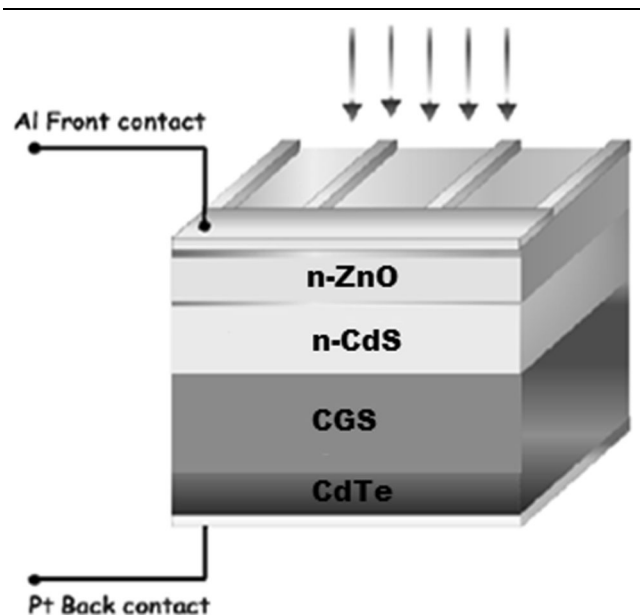$$FF = \frac{P_{max}}{P_t} = \frac{V_{max}I_{max}}{V_{OC}J_{SC}} \tag{1}$$

Fig. 1. Block diagram of CdTe/CGS/CdS/ZnO solar cell.

$$\text{PCE} = \frac{V_{\text{OC}} J_{\text{SC}} \text{FF}}{P_{\text{in}}} \qquad (2)$$

The parameters that need to be defined are absorber layer thickness, electron–hole mobility, intrinsic carrier concentration, electron affinity, band gap and doping density. For buffer and window layers similar parameters are also required which are listed in Table I. Where p and n are the hole and electron concentration in cm^{-3}, W is the thickness in μm. E_g is the band gap energy in eV, χ is the affinity in eV, N_V and N_C are the valence band and conduction band effective density of states in cm^{-3}, μe is the electron mobility in cm^2/Vs, and μp is the hole mobility in cm^2/Vs. All the simulations are conducted under AM 1.5 illumination (Table II).

RESULTS AND DISCUSSION

Energy Band Diagram

Band diagram for the structures of CdTe/CGS/CdS/ZnO and CGS/CdS/ZnO solar cells are represented in Figs. 2 and 3, respectively. These energy band diagrams are obtained for analysis from the SCAPS software. Energy band diagrams help in explaining the properties of both photovoltaic cells. For incident light photons the value that is optimal for most of the light to be absorbed for effective conversion efficiency is equal or greater than the maximum value in 1.4 eV.

$J − V$ Characteristics of CdTe/CGS/CdS and CGS/CdS Solar Cells

The function of the photovoltaic solar cell is to convert the energy of light into electricity. In light illumination, the photovoltaic cell starts working and current flows due to charge carriers produced by incident photons. Figure 4 explains the comparison of the $J − V$ characteristic curve of CdTe/CGS/CdS and CGS/CdS solar cells. In the proposed device, the thickness of the CGS absorber layer is 4 μm, and band gap energy is 2.2 eV. As CGS has a wide band gap absorber layer, the full light

spectrum is not absorbed. The band gap of CdTe is 1.45 eV which is smaller than CGS. So, CdTe helps to absorb light of a smaller photon energy than CGS because of its smaller band gap, and due to this, open circuit voltage (V_{oc}) and short-circuit current (J_{sc}) of the solar cell increases. This will also increase the overall power conversion efficiency and fill factor of a solar cell.

Effect of CdTe Back Surface Field Layer Thickness

Influence of CdTe with a BSF layer on the performance of the proposed device is explored and analyzed and shown in Fig. 5. The thickness of the BSF layer was changed while all remaining other parameters of the solar cell were kept constant. The thickness of the CdTe BSF layer was varied from 0.1 μm to 1 μm. Simulated fallouts show that with an increase in the thickness of the BSF layer, there is a very small change observed in functional parameters, i.e., in short-circuit current (J_{sc}), open circuit voltage (V_{oc}), power conversion efficiency (PCE) and the fill factor (FF). So, this result is comprehended such that an increase in BSF layer thickness does not affect the output of the proposed device. For the designing of CdTe/CGS/CdS solar cells, optimum thickness of the BSF layer is taken as 0.2 μm.

Effect of CGS Absorber Layers Thickness

Simulated fallouts on the influence of CGS absorber layer thickness on functional parameters of the proposed solar cell are shown in Fig. 6. The thickness of CGS changes from 1 μm to 10 μm. It is well understood from Fig. 6 that with an increase in the thickness of CGS absorber layers, conversion efficiency increases with FF and V_{oc}. But after reaching an optimal thickness, the fill factor starts to decrease with increase in thickness, whereas conversion efficiency, J_{sc} and V_{oc} are almost constant. To give an efficient output from a solar cell, the optimum thickness value for CGS is 3 μm.

Table I. Simulation parameters

Parameters	p⁺-CdTe (BSF layer)	p-CGS (Absorber)	n-CdS (Buffer)	n-ZnO (Window)
Thickness, W (μm)	0.1–2	1–4	0.1	0.1
Bandgap, E_g (eV)	1.45	2.2	2.42	3.35
Electron affinity, χ (eV)	4.28	4.5	4.4	4.5
Dielectric permittivity, ε_r	9.4	13.6	10	9
Effective Density of states, NC (cm^{-3})	8×10^{17}	2.2×10^{17}	2.2×10^{18}	2.2×10^{18}
Effective Density of states, NV (cm^{-3})	1.8×10^{19}	1.8×10^{18}	1.7×10^{19}	1.8×10^{19}
Electron mobility, μ_e (cm^2/Vs)	1050	100	340	100
Hole mobility, μ_p (cm^2/Vs)	100	25	50	25
Electron and hole concentration, n, p (cm^{-3})	1×10^{18}	1×10^{16}	1×10^{17}	1×10^{18}

Table II. Interface defects (neutral)

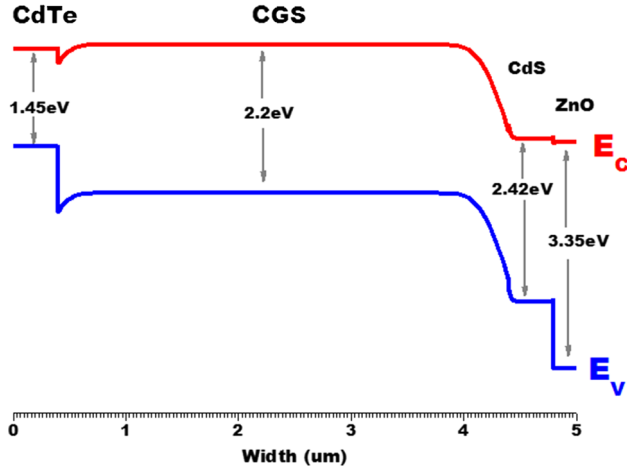| Defect layer properties	p⁺-CdTe/p-CGS	p-CGS/n-CdS
Capture cross-section area of electron/hole	1.0×10^{-15} cm^2	1.0×10^{-15} cm^2
Density of defect	1.0×10^{13} cm^{-2}	1.0×10^{13} cm^{-2}
Recombination velocity for electron and hole (S)	1.0×10^5 cm/s	1.0×10^5 cm/s

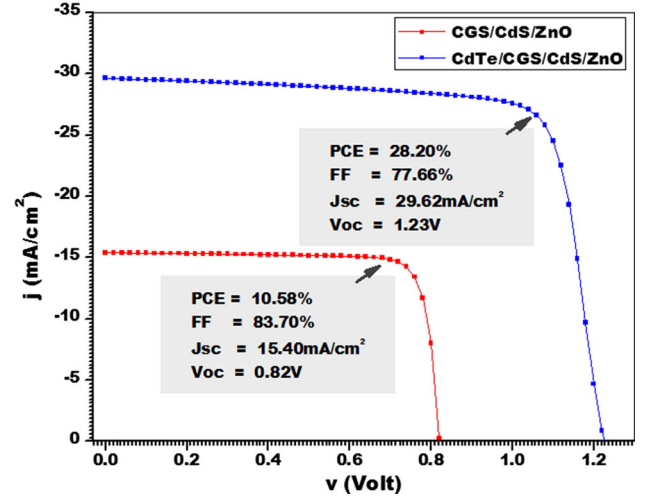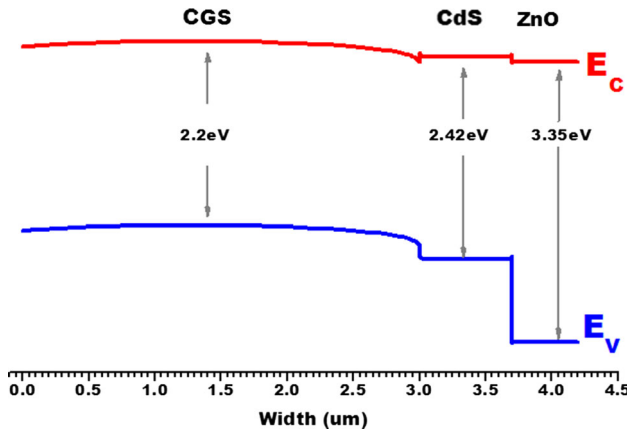Fig. 2. Energy band diagram of CdTe/CGS/CdS/ZnO solar cell.

Fig. 4. $J - V$ characteristics.
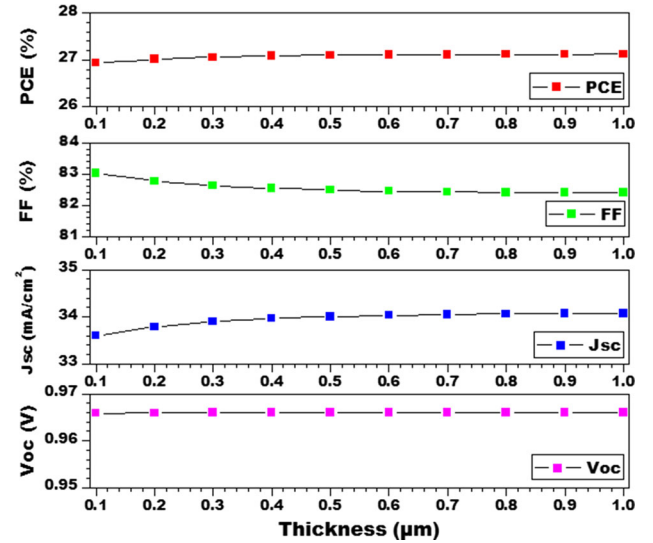

Fig. 3. Energy band diagram of CGS/CdS/ZnO solar cell.

Fig. 5. Thickness of CdTe BSF layer.

Effect of Absorber and BSF Layers Carrier Concentration

The phenomenon can be well understood from the PN junction model, which is expressed in Eqs. 3 and 4.

$$I_o = Aqn_i^2\left(\frac{D_e}{L_e N_A} + \frac{D_h}{L_h N_D}\right) \quad (3)$$

$$V_{oc} = \frac{kT}{q}\ln\left(\frac{I_L}{I_0} + 1\right) \quad (4)$$

In the above equations N_A and N_D are the acceptor and donor doping concentrations, respectively, D is the diffusion coefficient, k is the Boltzmann's constant, T is the temperature, L is diffusion length, q is the electron charge, I_0 is the saturation current, I_L is the current generated from
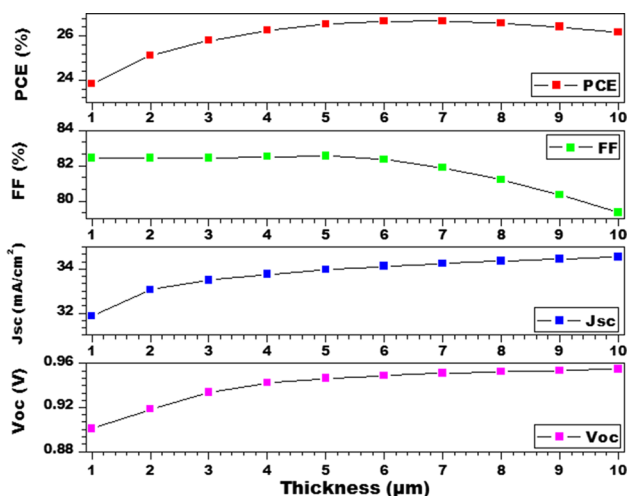
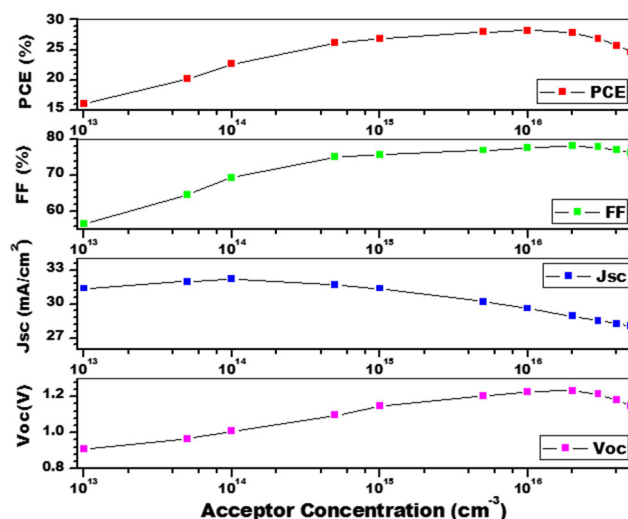Fig. 6. Thickness of CGS absorber layer.

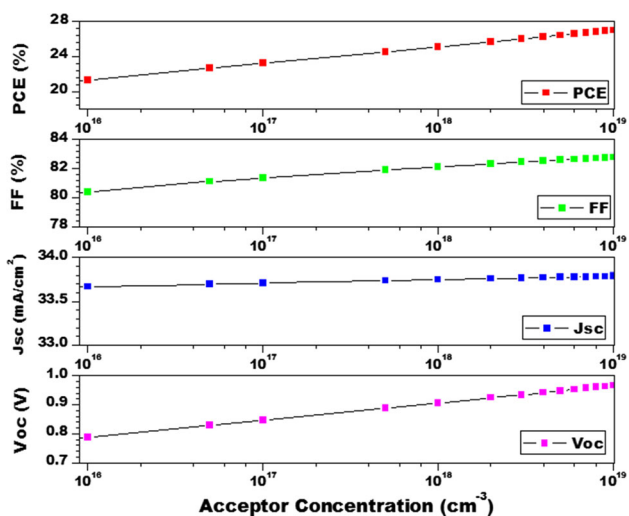Fig. 8. Acceptor concentration of CGS absorber layer.

Fig. 7. Acceptor concentration of CdTe BSF layer.

the light and A is the diode quality factor. e and h subscripts refer to electrons and holes, respectively. I_0 is reduced due to increase in absorber carrier concentration N_A and resultantly V_{oc} increases. However, with an increase in carrier concentration, short-circuit current J_{sc} decreases. This mainly happens since the recombination process is enhanced by the higher carrier densities and also reduces the probability of the collection of the photo-generated electrons. The higher wavelength photons will be deeply absorbed in CGS and CdTe layers; therefore, the conversion efficiency of the generation of electrons is dependent on the influence of diffusion.

The impact of carrier concentration on CdTe BSF and CGS absorber layers is shown in Figs. 7 and 8, respectively. Figure 7 illustrates that acceptor concentration of the CdTe BSF layer varies from 1×10^{16} cm^{-3} to 1×10^{9} cm^{-3}. Open circuit voltage

(V_{oc}), fill factor (FF) and power conversion efficiency (PCE) of proposed cells are increased with increase in the carrier concentration, whereas there is almost no change found in short-circuit current (J_{sc}). To give an efficient output from a solar cell, the optimum value of CdTe BSF layer carrier concentration is 4×10^{18} cm^{-3}.[31,32]

Figure 8 shows the acceptor concentration of the CGS absorber layer varies from 1×10^{13} cm^{-3} to 1×10^{17} cm^{-3}. With the increase of absorber doping concentration, open circuit voltage (V_{oc}), fill factor (FF) and power conversion efficiency increases, whereas J_{sc} decreases with the increase of concentration in CGS. After reaching the optimum value of acceptor carrier concentration, all functional parameters will be decreased. To give an efficient output from a solar cell, the optimum value of CGS absorber layer carrier concentration is 5×10^{16} cm^{-3}.

Effect of Buffer Layer Thickness

The influence of the thickness of the CdS buffer layer on a performance of the photovoltaic solar cell is explored in this step. The thickness of the CdS layer is changed from 0.01 μm to 0.1 μm and simulation results are illustrated in Fig. 9. From Fig. 9, it is clear that, although in the increase of buffer layer thickness, there is no change in open circuit voltage (V_{oc}). Whereas in short-circuit current (J_{sc}), power conversion efficiency (PCE) and fill factor (FF) are constant up to the optimal value. After reaching the optimal thickness value, then PCE, FF and J_{sc} are decreased. The optimized and the preferred thickness of a buffer layer is 0.05 μm.

Effect of Buffer Layer Carrier Concentration

The donor concentration simulation results are shown in Fig. 10. Donor concentration is varied from 1×10^{15} cm^{-3} to 1×10^{18} cm^{-3}, Fig. 10 shows
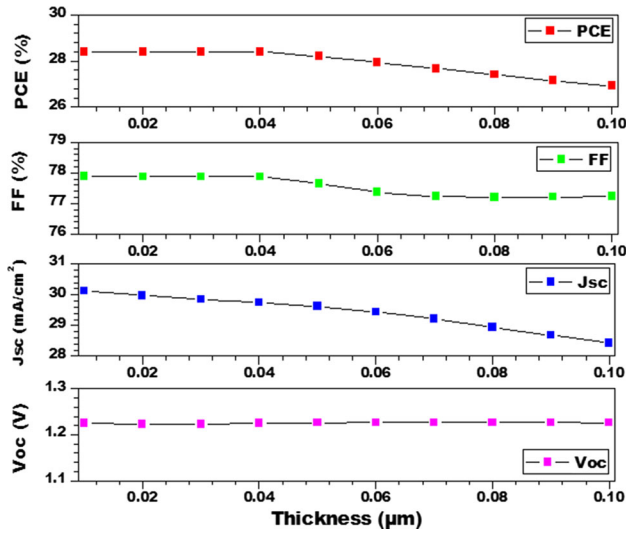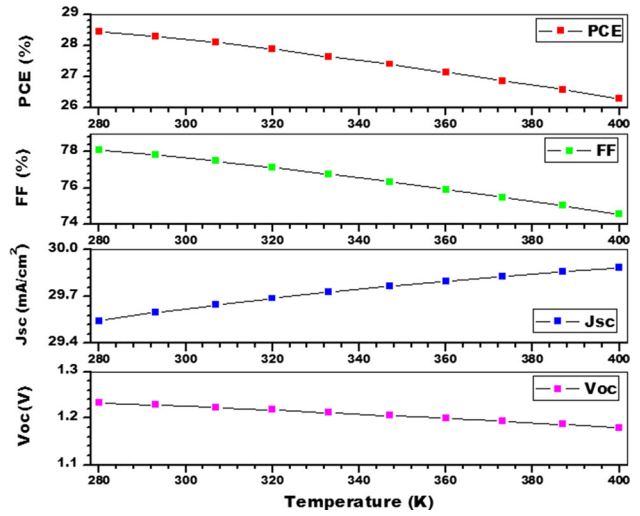
Fig. 9. Thickness of CdS buffer layer.

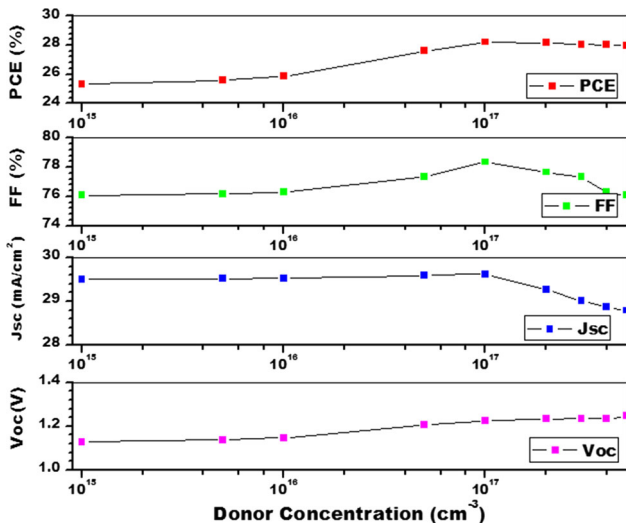Fig. 11. Temperature effect on cell performance.

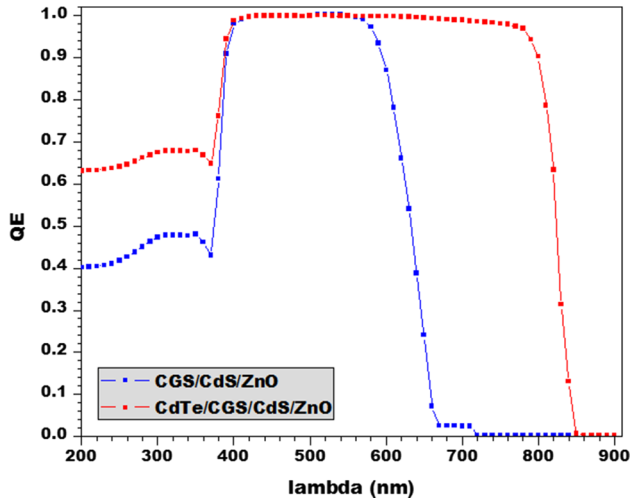Fig. 10. Donor concentration of CdS buffer layer.

Fig. 12. Quantum Efficiency.

that with an increase in donor concentration, power conversion efficiency (PCE) of a proposed solar cell increases, this change is small but not negligible. Figure 10 illustrates that with an increase in the donor concentration of a buffer layer, there is very small increase in open circuit voltage (V_{oc}), short-circuit current (J_{sc}) and in fill factor (FF). After reaching the optimal value of donor carrier concentration, PCE and FF are constant and J_{sc} decreases. If we further increase the concentration, PCE and FF will be decreased. To give an efficient output from a solar cell, the optimum value of CdS buffer layer carrier concentration is 1×10^{17} cm^{-3}.

Effect of Working Temperature on Performance of a Solar Cell

On the performance of a solar cell, working temperature plays an important role. The

photovoltaic panels are installed in the open air. The influence of the working temperature on the proposed cell is also investigated. For investigation of the performance of a cell, we take the temperature in a range from 280 K to 400 K. The simulation results are shown in Fig. 11. With the increase in temperature, cell performance decreases. Due to higher temperature the material carrier concentration, band gaps, electron and hole mobilities are affected and lower conversion efficiency from a cell is achieved.[33] Reverse saturation current depends on the temperature and, due to this, V_{oc} decreases with increase in temperature. Reverse saturation current increases with increase in temperature, and this decrease of current is the main cause of the V_{oc} decrease. Electrons gain more energy from the increased operating temperature. These electrons are unstable due to the higher temperature and are

Table III. Results

Parameters	CGS/CdS/ZnO (traditional cell)	CdTe/CGS/CdS/ZnO (proposed cell)
Conversion efficiency, PCE (%)	10.58	28.20
Fill factor, FF (%)	83.70	77.66
Short circuit current, J_{sc} (mA/cm^2)	15.40	29.62
Open circuit voltage, V_{oc} (Volts)	0.82	1.22

more likely to recombine with the holes before reaching the depletion region. Figure 11 illustrates that with the increase of temperature, conversion efficiency decreases. FF, V_{oc} also decrease along with the increase in temperature, whereas J_{sc} increases.

Quantum Efficiency of a CdTe/CGS/CdS PV Solar Cell

Figure 12 explains the quantum efficiency (QE) of a proposed photovoltaic solar cell in comparison with CdS/CGS. For the CGS/CdS/ZnO structure, QE reached a maximum between 400 nm and 570 nm with decreases for large wavelengths, and it vanishes at 680 nm. This is related to the absorption coefficient used for CGS, which diminishes gradually from 570 nm to 680 nm. By adding a CdTe absorber layer, absorption coefficient increases and gives higher efficiency. CdTe as a stacked absorber layer gives a radical fall in quantum efficiency above 800 nm.

By using CdTe as a back surface field layer, the overall efficiency of a photovoltaic solar cell increases. This is well understood from Table III. Open circuit voltage (V_{oc}), increases from 0.82 V to 1.22 V; short circuit current (J_{sc}) improves from 15.40 mA/cm^2 to 29.62 mA/cm^2, Fill factor changes from 83.70% to 77.66% and conversion efficiency of a thin film photovoltaic solar cell increases from 10.58% to 28.20%. Table III shows the results of the comparison of two modeled solar cells in SCAPS. From Table III it is clear that CdTe/CGS/CdS/ZnO has higher conversion efficiency than that of CGS/CdS/ZnO due to its ability to absorb photons below the CGS band gap.

CONCLUSION

Thin film solar cell structure with physical operating features is described by different software. In this research work, we have performed the detailed analysis of a solar cell on SCAPS for a better understanding of solar cell behavior. In-depth understanding of a solar cell's $J - V$ characteristic measures is not enough to fully describe its behavior, because behavior or response of a solar cell also depends on its internal physical mechanism. In this work, the performance of a CdTe/CGS/CdS in comparison to a CGS/CdS photovoltaic solar cell is simulated and analyzed on SCAPS simulator software. The values obtained from the proposed solar cell are the power conversion efficiency (PCE) of 28.20%, fill factor (FF) 77.66%, short circuit current (J_{sc}) 29.62 mA/cm^2 and open circuit voltage (V_{oc}) 1.22 V. The results will give important guidelines for the feasible fabricating of higher efficiency CdTe based solar cells. From the results, it is clear that, to attain improved performance from solar cells, numerical modeling plays a significant role.

REFERENCES

1. Y.H. Khattak, T. Mahmood, K. Alam, T. Sarwar, I. Ullah, and H. Ullah, *Am. J. Electr. Power Energy Syst.* (2014). https://doi.org/10.11648/j.epes.20140305.11.
2. I. Rimmaudo, A. Salavei, and A. Romeo, *Thin Solid Films* (2013). https://doi.org/10.1016/j.tsf.2012.11.113.
3. M.A. Green, K. Emery, Y. Hishikawa, W. Warta, and E.D. Dunlop, *Prog. Photovolt. Res. Appl.* (2015). https://doi.org/10.1002/pip.2573.
4. M. Elbar, S. Tobbeche, and A. Merazga, *Sol. Energy* (2015). https://doi.org/10.1016/j.solener.2015.08.029.
5. J.D. Major, R. Tena-Zaera, E. Azaceta, L. Bowen, and K. Durose, *Sol. Energy Mater. Sol. Cells* (2017). https://doi.org/10.1016/j.solmat.2016.10.024.
6. E.S. Cha, Y.M. Ko, S.C. Kim, and B.T. Ahn, *Curr. Appl. Phys.* (2017). https://doi.org/10.1016/j.cap.2016.10.014.
7. R.W. Crisp, G.F. Pach, J.M. Kurley, R.M. France, M.O. Reese, S.U. Nanayakkara, B.A. Macleod, D.V. Talapin, M.C. Beard, and J.M. Luther, *Nano Lett.* (2017). https://doi.org/10.1021/acs.nanolett.6b04423.
8. Y. Chen, X. Tan, S. Peng, C. Xin, A.E. Delahoy, K.K. Chin, and C. Zhang, *J. Electron. Mater.* (2018). https://doi.org/10.1007/s11664-017-5850-9.
9. P.Y. Su, C. Lee, G.C. Wang, T.M. Lu, and I.B. Bhat, *J. Electron. Mater.* (2014). https://doi.org/10.1007/s11664-014-3142-1.
10. S. Wang, T. Nazuka, H. Hagiya, Y. Takabayashi, S. Ishizuka, H. Shibata, S. Niki, M.M. Islam, K. Akimoto, and T. Sakurai, *J. Electron. Mater.* (2018). https://doi.org/10.1007/s11664-018-6120-1.
11. A. Romeo, M. Terheggen, D. Abou-Ras, D.L. Bätzner, F.-J. Haug, M. Kälin, D. Rudmann, and A.N. Tiwari, *Prog. Photovolt. Res. Appl.* (2004). https://doi.org/10.1002/pip.527.
12. S. Ullah, M. Mollar, and B. Marí, *J. Solid State Electrochem.* (2016). https://doi.org/10.1007/s10008-016-3237-0.
13. X. Peng, M. Zhao, D. Zhuang, L. Guo, L. Ouyang, R. Sun, L. Zhang, Y. Wei, S. Zhan, X. Lv, Y. Wu, and G. Ren, *J. Alloys Compd.* (2017). https://doi.org/10.1016/j.jallcom.2017.02.016.
14. M. Mazzer, S. Rampino, G. Spaggiari, F. Annoni, D. Bersani, F. Bissoli, M. Bronzoni, M. Calicchio, E. Gombia, A. Kingma, F. Pattini, and E. Gilioli, *Sol. Energy Mater. Sol. Cells* (2017). https://doi.org/10.1016/j.solmat.2016.10.048.

15. A. Gerthoffer, C. Poulain, F. Roux, F. Emieux, L. Grenet, and S. Perraud, *Sol. Energy Mater. Sol. Cells* (2017). https://doi.org/10.1016/j.solmat.2016.11.022.

16. X. Wu, *Sol. Energy* (2004). https://doi.org/10.1016/j.solener.2004.06.006.

17. K. Ramanathan, M.A. Contreras, C.L. Perkins, S. Asher, F.S. Hasoon, J. Keane, D. Young, M. Romero, W. Metzger, R. Noufi, J. Ward, and A. Duda, *Prog. Photovolt. Res. Appl.* (2013). https://doi.org/10.1002/pip.494.

18. M. Mezher, R. Garris, L.M. Mansfield, K. Horsley, L. Weinhardt, D.A. Duncan, M. Blum, S.G. Rosenberg, M. Bär, K. Ramanathan, and C. Heske, *Prog. Photovolt. Res. Appl.* (2016). https://doi.org/10.1002/pip.2764.

19. W. Wang, J. Yang, X. Zhu, and J. Phillips, *Front. Optoelectron. China* (2011). https://doi.org/10.1007/s12200-011-0151-z.

20. W. Shockley and H.J. Queisser, *J. Appl. Phys.* (1961). https://doi.org/10.1063/1.1736034.

21. S. Ullah, H. Ullah, F. Bouhjar, M. Mollar, and B. Marí, *Sol. Energy Mater. Sol. Cells* (2017). https://doi.org/10.1016/j.solmat.2017.06.062.

22. O.D. Miller, E. Yablonovitch, and S.R. Kurtz, *IEEE J. Photovolt.* (2012). https://doi.org/10.1109/JPHOTOV.2012.2198434.

23. Y.H. Khattak, F. Baig, H. Toura, S. Ullah, B. Marí, S. Beg, and H. Ullah, *Curr. Appl. Phys.* (2018). https://doi.org/10.1016/j.cap.2018.03.013.

24. F. Baig, H. Ullah, Y.H. Khattak, and B. Mari Soucase, *Int. Renew. Sustain. Energy Conf. IEEE.* (2016). https://doi.org/10.1109/irsec.2016.7983899.

25. Y.H. Khattak, F. Baig, S. Ullah, B. Marí, S. Beg, and H. Ullah, *Optik (Stuttg)* (2018). https://doi.org/10.1016/j.ijleo.2018.03.055.

26. N. Khoshsirat and N.A. Md, Yunus. *J. Electron. Mater.* (2016). https://doi.org/10.1007/s11664-016-4744-6.

27. A. Chihi, M.F. Boujmil, and B. Bessais, *J. Electron. Mater.* (2017). https://doi.org/10.1007/s11664-017-5547-0.

28. P.Y. Su, R. Dahal, G.C. Wang, S. Zhang, T.M. Lu, and I.B. Bhat, *J. Electron. Mater.* (2015). https://doi.org/10.1007/s11664-015-3829-y.

29. A. Niemegeers and M. Burgelman, *Conf. Rec. Twenty Fifth IEEE Photovolt. Spec. Conf.* (1996). https://doi.org/10.1109/pvsc.1996.564274.

30. K. Decock, P. Zabierowski, and M. Burgelman, *J. Appl. Phys.* (2012). https://doi.org/10.1063/1.3686651.

31. V. Barrioz, Y.Y. Proskuryakov, E.W. Jones, J.D. Major, S.J.C. Irvine, K. Durose, and D.A. Lamb, *MRS Proc.* (2007). https://doi.org/10.1557/PROC-1012-Y12-08.

32. S. Oehling, H.J. Lugauer, M. Schmitt, H. Heinke, U. Zehnder, A. Waag, C.R. Becker, and G. Landwehr, *J. Appl. Phys.* (1996). https://doi.org/10.1063/1.361160.

33. M.S. Hossain, N. Amin, M.A. Matin, M.M. Aliyu, T. Razykov, and K. Sopian, *Chalcogenide Lett.* 8 (4), 263 (2011).